

## Some theoretical predictions on the relationships among spreading rate, mantle temperature, and crustal thickness

Wusi Su,<sup>1</sup> Carolyn Z. Mutter, John C. Mutter,<sup>1</sup> and W. Roger Buck<sup>1</sup>

Lamont-Doherty Earth Observatory of Columbia University, Palisades, New York

A series of numerical experiments on mantle flow and melting predict a positive relation between mantle temperature and crustal thickness. The models also demonstrate that crust formed at slow spreading rates is more sensitive to variations in mantle temperature than crust formed at fast rates so that the range of calculated thicknesses is much greater for crust formed at slower rates. An instantaneous mantle temperature increase results in a transient pulse of melt production that is also more pronounced at slower spreading rates. The predicted behavior is caused by the interplay between mantle flow driven by plate separation and that driven by thermal, compositional, and melt-related buoyancy. A temperature increase results in a decrease in mantle viscosity and an increase in the depth at which melting begins. A lower viscosity leads to stronger buoyancy-driven flow that carries more mantle to shallow depths below the ridge. Thermal buoyancy effects, which may result in cooling and mixing of depleted and undepleted material under the ridge, appear to be of greater importance at slower spreading rates. The steady state results are broadly consistent with global compilations of oceanic crustal thickness that show larger variations in crustal thickness at slower spreading rates than at faster rates. Thicknesses estimated from seismic refraction data from crust formed within a single segment of the Mid-Atlantic Ridge but at different spreading rates (1.0 to 1.9 cm/yr) are consistent with (but do not prove) the model results. The transient pulse of melt production associated with a rapid increase in mantle temperature might occur when a ridge becomes proximal to a hot spot.

### INTRODUCTION

It is widely conceded that the total thickness and gross layer structure of oceanic crust derived from seismic refraction measurements appears to be almost insensitive to changes in spreading rate [White, 1984; White *et al.*, 1992]. A recent compilation of crustal thickness estimates made during the past two decades using data collected away from elevated plateaus [Chen, 1992] shows no systematic change in crustal thickness with spreading rate. Instead, the data show large variations in crustal thickness at slow spreading rates and comparatively smaller variations in thickness for crust produced at faster rates (Figure 1).

Oceanic crust created at spreading centers is the result of pressure release partial melting of mantle that upwells beneath ridges as a consequence of plate separation [e.g., Oxburgh, 1980]. While faster spreading must lead to a greater amount of melting, the implication of a constant crustal thickness is that the amount of melt produced per unit of plate separation is also constant. These processes can be simulated in numerical experiments on partial melting and melt migration in the mantle [Ribe, 1985; Spiegelman and McKenzie, 1987; Phipps Morgan, 1987; Scott and Stevenson, 1989; Buck and Su, 1989;

Sotin and Parmentier, 1989; Su and Buck, 1993; Cordery and Phipps Morgan, 1993] and can test the possible importance of various processes that contribute to the formation of crust. By contrast to the implications of observational studies, several recent numerical simulations suggest that for a reasonable range of mantle parameters, a systematic relationship between crustal thickness and spreading rate should exist. For example, Reid and Jackson [1981], who considered only passive, plate-driven flow, saw a large decrease in crustal thickness with decrease in spreading rate. More recently, Sotin and Parmentier [1989] and Su and Buck [1993] showed that buoyancy-driven flow might influence the dependence of crustal thickness on spreading rate.

In this contribution we examine numerical predictions of the dependence of crustal thickness on several mantle parameters, with an emphasis on temperature and spreading rate. We then attempt to match model predictions to the results of marine seismic experiments that are sufficiently well controlled that they might test the theoretical predictions. We find that few data of this type exist; analysis of a moderately well constrained data set does not lead to a very compelling test of the model predictions.

### NUMERICAL MODEL FORMULATION

Crustal thicknesses were calculated from each of a series of two-dimensional numerical experiments with varying mantle parameters and different boundary conditions. The numerical experiments model the effects of buoyancy driven mantle flow [Su and Buck, 1993; Scott and Stevenson, 1989; Sotin and Parmentier, 1989] derived in the following way. Buoyancy is caused by the effects of thermal expansion, compositional

<sup>1</sup>Also at Department of Geological Sciences, Columbia University, New York.

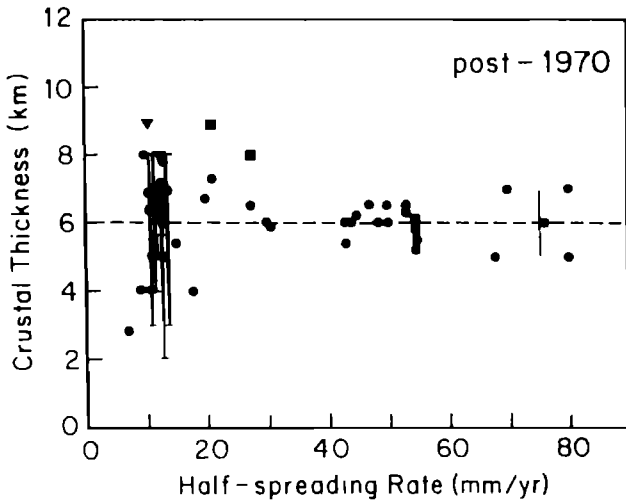


Fig. 1. Crustal thickness versus spreading rate from seismic studies conducted after 1970 [from *Chen, 1992*]. Crustal thicknesses are represented as solid dots; fracture zone data are presented as solid dots with an error bar. Data collected near hot spots or thought to be influenced by other complications are shown as solid triangles and squares, respectively. Although the average crustal thicknesses seems to remain constant (dashed line), the data also show large variations in thickness of crust produced at slower rates of seafloor spreading compared to crust produced at faster rates.

variation created by melt extraction, and the phase change associated with partial melting. We consider a model box filled with viscous fluid to represent a cross-sectional area of the mantle including a spreading center (Figure 2). The right side of the box is a symmetric boundary representing a vertical

surface passing through a ridge crest. At this boundary there is no lateral flow of material or heat. The surface is made to move horizontally at a constant velocity except in the region close to the ridge crest where a cosine taper is utilized to reduce the velocity to zero over a distance of 5 km. The temperature at the surface is held constant at 0°C. The base of the lithosphere is defined by the 1050°C isotherm. At the left and bottom boundaries of the box, free and fixed flow boundary conditions were applied in different cases. In the case of free flow boundary conditions, material is allowed to pass through the boundaries of the box where the viscous normal stress and the vorticity are specified to be zero. For fixed flow boundary conditions, the boundary flow field is specified as the steady state pattern of flow for plate-driven flow without buoyancy forces. The temperature  $T_m$  of the material that flows into the box from below was varied from 1275°C to 1375°C in different model runs. At the left side there is no lateral conduction of heat. The viscosity  $\mu$  within the box is related to temperature  $T$  by a standard relation

$$\mu(T) = \mu_0 \exp[(E/R)(1/T - 1/T_m)]$$

where  $R$  is the universal gas constant, the activation energy,  $E$ , is set at 420 kJ/mol and the viscosity,  $\mu_0$ , (when  $T = T_m$ ) is assumed to be  $10^{18}$ ,  $10^{19}$ , and  $10^{20}$  Pa s for different cases. Average mantle viscosity cannot be much lower because thermal convection causes rapid cooling if the viscosity is much lower than  $10^{19}$  Pa s [*Su and Buck, 1993*] except in the region of larger melt fraction [*Borch and Green, 1990*]. Following *Richter and McKenzie [1984]* and others, we adopt a power law relation between porosity  $\phi$  and permeability  $k$ ; namely,  $k = (a^2/b) \cdot \phi^2$ , where  $a$  is the grain size and  $b$  is a constant which has been estimated to be about 3000 for

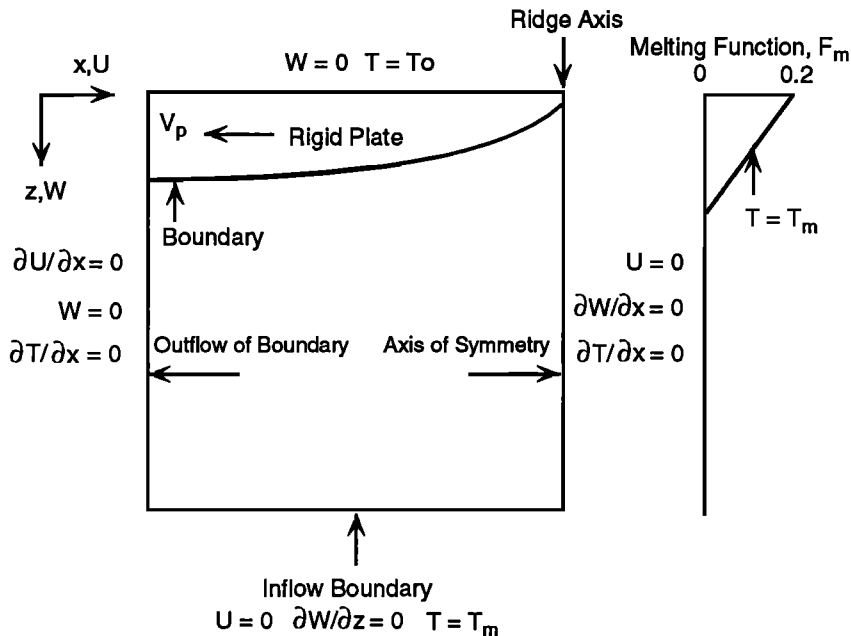


Fig 2. Left: schematic of model used for numerical experiments.  $x$  and  $z$  represent the horizontal and vertical axes of a coordinate system shown in top left corner.  $U$  and  $W$  are velocities in the directions of  $x$  and  $z$  respectively.  $T$  represents temperature. The right side of the box is a symmetric boundary representing a vertical surface passing through a ridge crest. At this boundary there is no lateral flow of material or heat. The surface is made to move horizontally at a constant velocity  $V_p$ . The temperature at the surface is held constant at  $T_0$ . The base of the lithosphere is defined by 1050°C isotherm. Free flow across left (outflow) and bottom (inflow) boundaries represents the calculations shown in Figures 3-6.  $T_m$  is the temperature of the material that flows into the box. Right: schematic of melt function, assumed to follow a simple linear relation with temperature and pressure above the solidus.

ultramafic partial melts [Cheadle, 1989]. The melting function is assumed to follow a simple linear relation with temperature and pressure above the solidus  $F_m(T,p) = (T-1180-0.06p)/600$ . Energy changes due to latent heat and frictional heating between matrix and melt are ignored. Including the latent heat term would lower temperature with height above the base of the melting region. Thus our crustal thicknesses, determined by dividing the calculated volumetric rate of melt production by the spreading rate, represent maximum estimates.

#### Free Flow Calculations

Calculations of crustal thickness as a function of mantle temperature for half spreading rates ( $V_p$ ) of 1 cm/yr and 5 cm/yr for free flow boundary conditions are shown in Figure 3. The axes are normalized to the point where the curves intersect (here mantle at a potential temperature of 1317°C forms 7-km-thick crust; this normalization scheme is also used for Figures 4-6). Figure 3 shows that crustal thickness increases with mantle temperature for both slow and fast spreading rates. However, the rate of increase for the case of a slow spreading rate is larger than that for the fast spreading rate. This implies that crustal formation at slow spreading rates is more sensitive to mantle temperature variations than crustal formation at faster rates. This property may account for the observed increase in scatter in the crustal thickness versus spreading rate compilation of Chen [1992] (Figure 1).

The point at which the curves in Figure 3 intersect depends on mantle parameters such as permeability and viscosity; the present calculation assumes a mantle of low permeability, corresponding to 0.2 mm grain size, and a reference viscosity of  $10^{19}$  Pa s (see also below). In this case, if the regional temperature of upwelling mantle is reduced below 1317°C

(negative  $\Delta T_m$ ) a greater thickness crust is produced for fast spreading than for slow spreading. The effect is opposite for potential temperatures greater than 1317°C (positive  $\Delta T_m$ ). Thus detailed interpretations of comparative relationships between crustal thickness and spreading rate at any mantle temperature also requires consideration of other mantle properties.

The effects of variations in mantle viscosity ( $\mu_0$ ) are shown in Figure 4. Higher viscosity results in a reduction in mantle flow into the region where melting occurs, so less melt is created and thinner crust is formed. Crustal thickness produced for  $\mu_0$  of  $10^{18}$  Pa s is larger than that at  $\mu_0$  of  $10^{19}$  Pa s (case of Figure 3), which is larger again than the crustal thicknesses for  $\mu_0$  of  $10^{20}$  Pa s. The curves for fast and slow spreading rates always intersect as they did in the initial calculation (Figure 3), but the point of intersection moves to higher temperatures as viscosity increases.

The physical phenomenon described by the curves in Figure 4 is the effect of buoyancy-driven flow on melt production [Scott, 1993; Su and Buck, 1993]. For any given set of mantle conditions, buoyancy-driven flow is more important at slow spreading rates [Su and Buck, 1993]. This effect is shown by the solid, steeper slope curve in Figure 4. Additionally, as viscosity increases, the mantle becomes increasingly resistant to flow. As a result, the slopes of each mantle temperature/crustal thickness curves reduce with increasing viscosity. At very high viscosity the curves exhibit less of a spreading rate dependence because the effect of buoyancy-driven flow on crustal production is suppressed.

The effect of variations in mantle permeability on the behavior of the system is illustrated in Figure 5. The two pairs of curves represent cases with small (0.2 mm grain size; case of Figure 3) and large (effectively infinite) permeabilities,

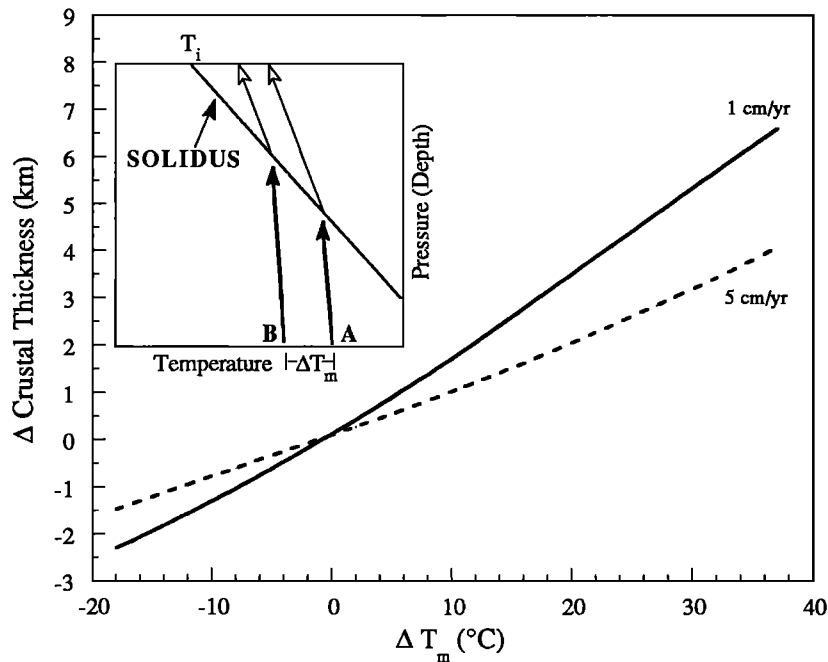


Fig. 3. Crustal thickness versus mantle temperature for half spreading rates of 1 cm/yr and 5 cm/yr. The calculations assume a small permeability (grain size 0.2 mm), moderate viscosity ( $\mu_0$  of  $10^{19}$  Pa s) mantle. The axes are normalized to the intersection point of the curves, where 7-km-thick crust formed from mantle at a potential temperature of 1317°C. Both lines show a positive relationship, indicating that crustal thickness increases with mantle temperature independent of spreading rate. However, the slope of the curve for the slow spreading rate is larger than that for the fast spreading rate; that is, crust formed at the slower rate appears to be more sensitive to variations in mantle temperature than crust formed at the faster rate.

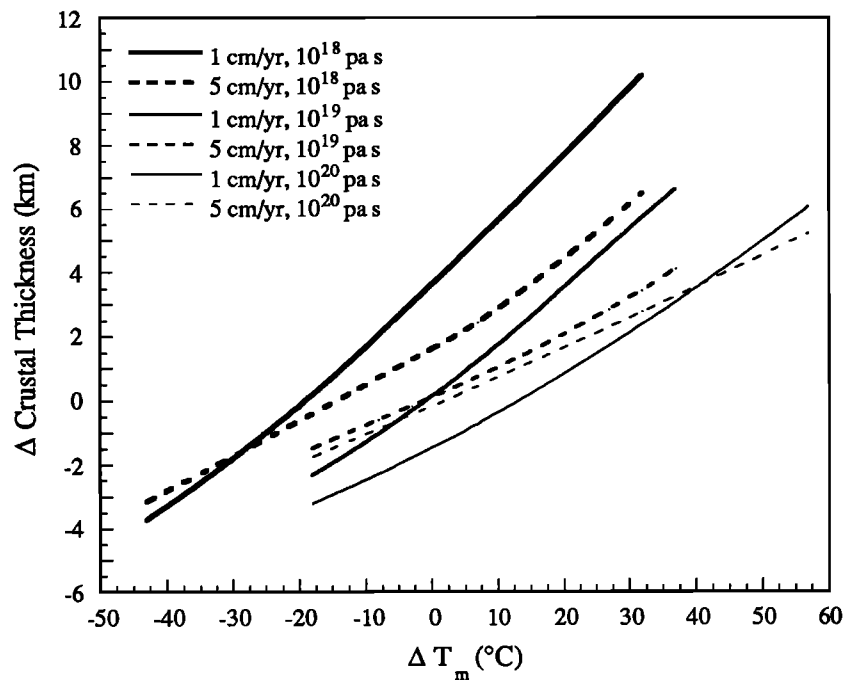


Fig. 4. The effects of variations in average viscosity ( $\mu_0$ ) on the relationship between crustal thickness and mantle temperature, normalized as in Figure 3. The three pairs of curves represent three different selections ( $10^{18}$  Pa s,  $10^{19}$  Pa s, and  $10^{20}$  Pa s) of  $\mu_0$ , the reference mantle viscosity ( $10^{19}$  Pa s case from Figure 3). Convection is resisted as viscosity increases, lessening the effect of spreading rate on crustal thickness.

respectively. While the relationship of increasing crustal thickness with increasing mantle temperature remains, the rate of increase lessens with increased permeability. The physical phenomenon relates to the effect of permeability on buoyancy. If all melt were extracted instantly because of very high mantle

permeability, buoyancy caused by the phase change associated with partial melting would be negligible. A reduction in buoyancy weakens upward flow of mantle in a way that is similar to the reduction in flow at higher mantle viscosity discussed above.

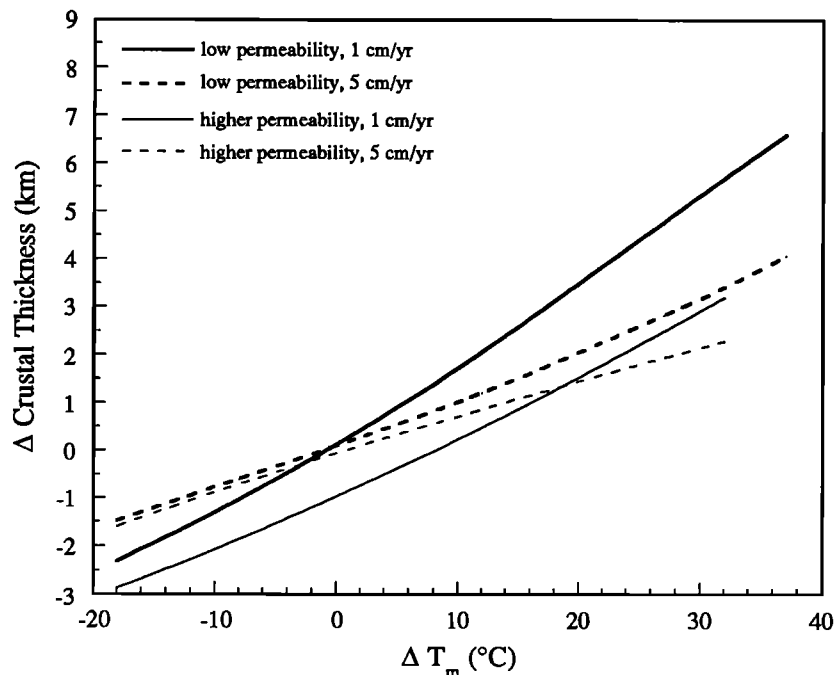


Fig. 5. The effect of permeability on the relationship between crustal thickness and mantle temperature, normalized as in Figure 3. Two pairs of curves represent small (grain size 0.2 mm, from Figure 3) and effectively infinite (instantaneous melt extraction) permeabilities. Buoyancy introduced by the phase change associated with partial melting is negligible for the case of infinite permeability. As a result, the flow of mantle and buoyancy-driven flow are weakened in a manner similar to the case of increasing viscosity (Figure 4).

Our initial calculations (Figure 3) illustrate a fundamental relationship between crustal thickness and mantle temperature for fast spreading and slow spreading rates and reasonable mantle properties. Using the same mantle parameters as calculations of Figure 3, we made a suite of calculations describing a greater range of spreading rates ( $V_p=0.5-7.5$  cm/yr) and illustrate the results in a different form by plotting crustal thickness as a function of spreading rate for different mantle temperatures (Figure 6). At slow spreading rates ( $V_p=0.5-1.0$  cm/yr) the curves are approximately parallel and show a strong dependence of crustal thickness on spreading rate for all but the highest mantle temperatures. At intermediate-to-fast rates ( $V_p=1.5-7.5$  cm/yr) the curves representing low to moderate mantle temperatures remain subparallel but span a smaller range of crustal thicknesses and show comparatively small gradients.

In the range of mantle temperatures associated with the formation of crust 5-7 km thick (e.g., lower curves of Figure 6) there is little change in crustal thickness for  $V_p$  greater than about 2.0 cm/yr. This range encompasses conditions for the production of much of the world's oceanic lithosphere and gives a potential explanation for the apparent global invariance of crustal thickness. However, at slower spreading rates and higher temperatures the behavior changes considerably. As spreading rates slow to less than 1 cm/yr (half rate) crustal thickness decreases rapidly for all but the highest mantle temperatures calculated. At higher mantle temperatures, crustal thickness exhibits a distinct dependence on spreading rate.

Stated differently, larger than normal crustal thicknesses can be achieved in two ways. One is the well understood effect of increasing mantle temperature. A second factor that increases

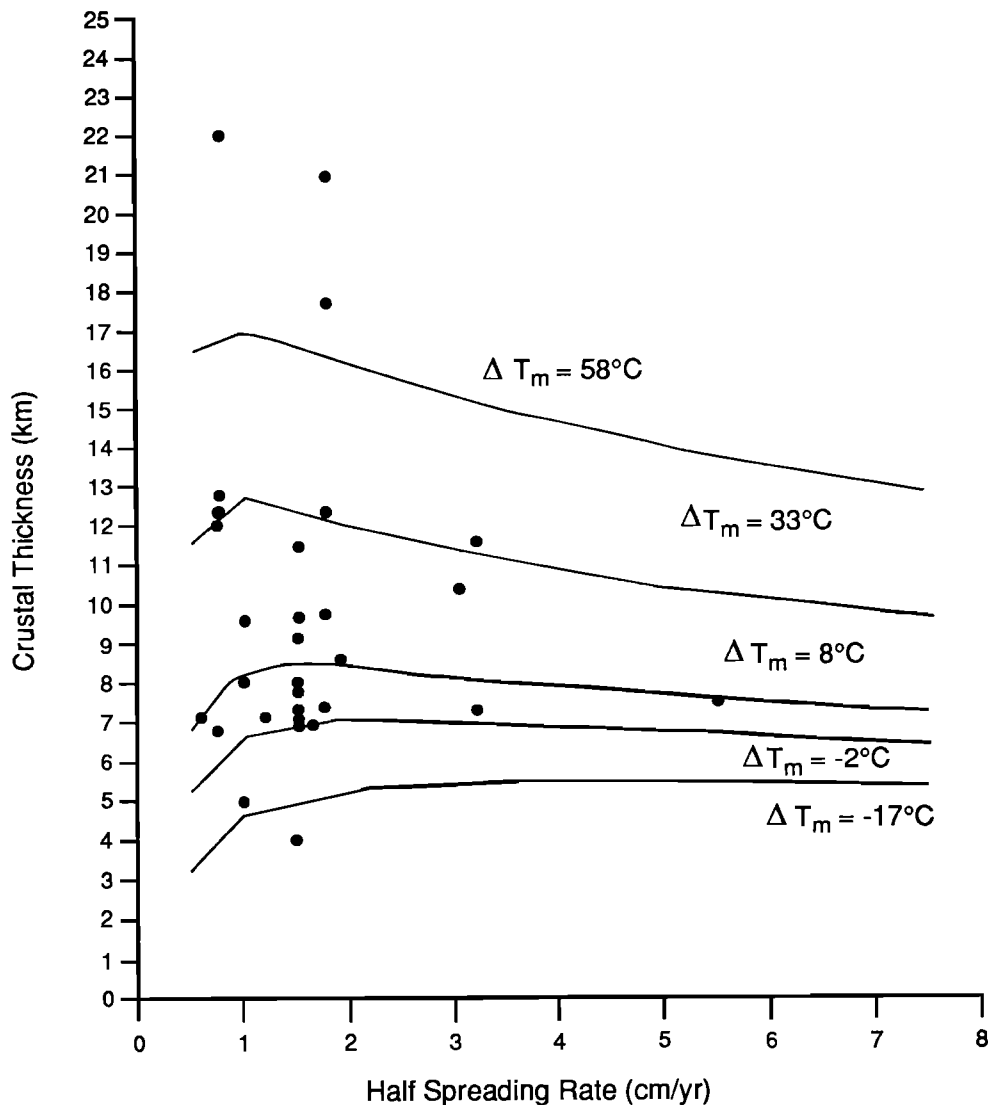


Fig. 6. Crustal thickness versus half spreading rates for different temperatures of mantle (curves from top to bottom represent  $\Delta T_m$  of 58°C, 33°C, 8°C, -2°C, and -17°C, respectively) calculated using the same conditions as Figure 3. Crustal thickness increases as a function of mantle temperature for all spreading rates but increases more rapidly for slower spreading rates. At the slowest spreading rates (0.5-1.0 cm/yr, half rate) the curve segments are nearly parallel and show the greatest increase in crustal thickness with temperature. At intermediate to fast spreading rates (2.0-7.5 cm/yr, half rate) the curve segments are subparallel and show a comparatively smaller gradient. Data values from the compilation of Mutter and Mutter [1993] are plotted on the same diagram and span the field of model curves, with most variation observed at slow spreading rates.

in importance at higher mantle temperatures results from the enhanced relative effect of buoyancy-driven flow at slower spreading rates. The results hold that for a given mantle temperature, crustal thickness generally increases as spreading rate decreases until a value of about 1.5 cm/yr is reached and then rapidly decreases. The effect of spreading rate on crustal thickness is more pronounced at higher mantle temperatures.

#### Considerations of Boundary Conditions and Buoyancy-Driven Flow

The model calculations presented here do not, by design, incorporate the effect of the entire convecting mantle. To resolve details of flow and melting that might be present under a ridge, we have limited the size of the numerical box considered. Different boundary conditions have been applied in different numerical methods. Solutions by Fourier

transformation are based on periodic boundary conditions. Some workers [e.g., Scott and Stevenson, 1989; Sotin and Parmentier, 1989; Scott, 1993] have used fixed-flow boundary conditions at the bottom of the box and at the side where material leaves the box. We have let the flow field determine how fast material enters and leaves the box. Neither our boundary conditions nor the fixed velocity conditions are entirely correct and can perhaps be considered end-members of a range of possibilities. Fixing boundary flow assumes that the buoyancy effects do not change the flow field outside of the box. For our boundary conditions, buoyancy can lead to more material flowing through the model box. However the temperature of the material flowing into the box is not affected by the buoyancy-driven flow.

To estimate the effects of different boundary conditions on our calculations, we performed several numerical experiments with and without buoyancy terms for both free and fixed flow

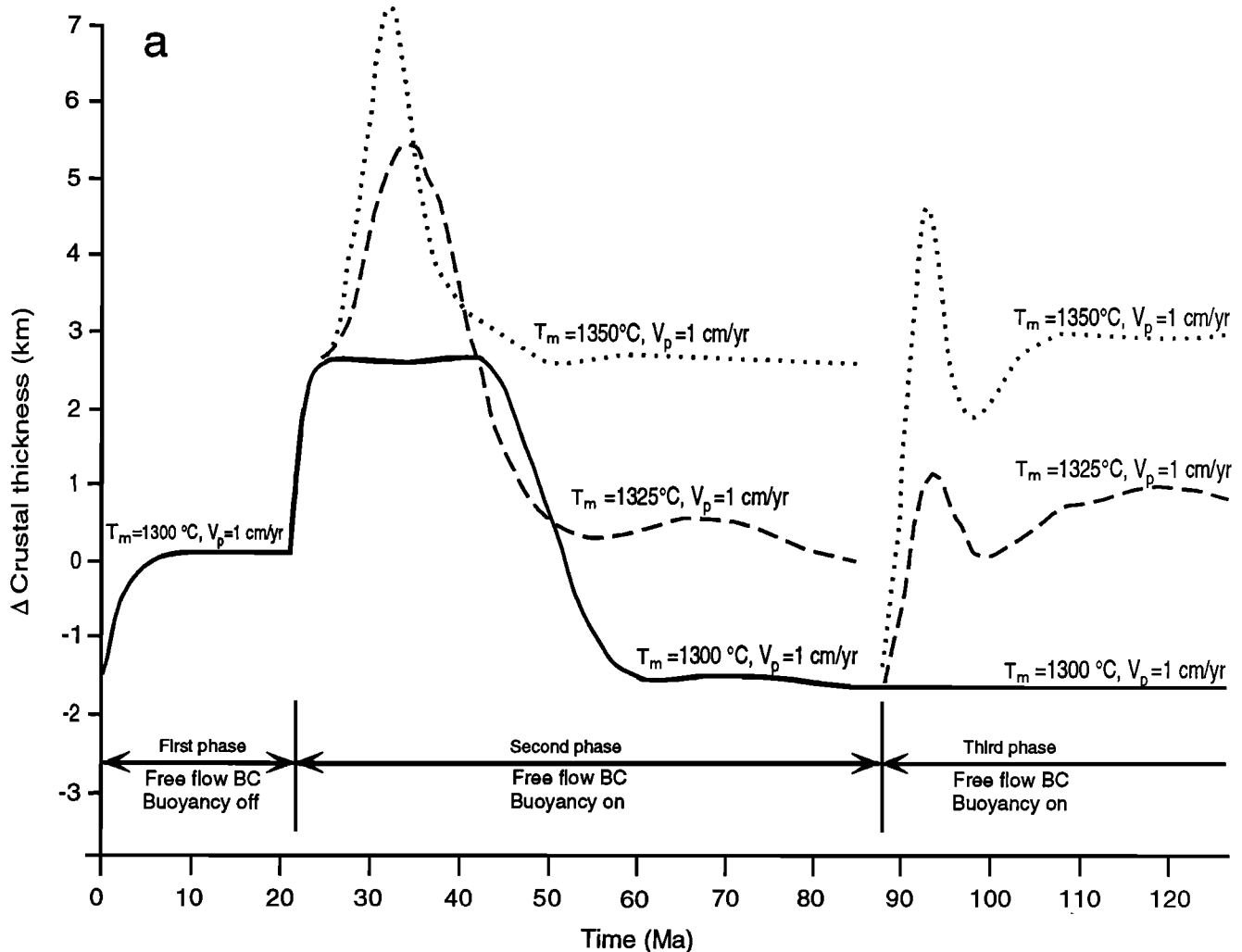


Fig. 7. Time series of crustal thickness calculations for slow (half rate 1 cm/yr, Figure 7a) and fast (half rate 5 cm/yr, Figure 7b) spreading rates ( $V_p$ ). Calculations were made in three phases. The first phase represents free flow boundary conditions (BC) with no buoyancy terms. Vertical axes are normalized to the steady state crustal thickness obtained at the end of phase one. Second phase calculations were initiated by fixing the steady state boundary flow determined from the first phase as boundary conditions and incorporate buoyancy-driven flow (solid line) and instantaneous input mantle temperature ( $T_m$ ) increases of 25°C (dashed line) and 50°C (dotted line). Calculations for a third phase were initiated by fixing boundary conditions as the steady state solution from the end of the second phase for the case of  $T_m=1300^\circ\text{C}$  (solid line) with instantaneous input mantle temperature increases of 25°C (dashed line) and 50°C (dotted line). Fluctuations in mantle melt and flow have a greater influence on crust formed at slower spreading rates. Transient effects, observed at the initiation of the second and third phases, are more pronounced at slower spreading rates and higher mantle temperatures. Please see text for further discussion.

boundary conditions and for slow and fast spreading cases ( $V_p$  of 1 cm/yr, Figure 7a; and 5 cm/yr, Figure 7b). The calculations were done as a time series in three phases. In the first phase, a flow field is created purely by plate separation (mantle is allowed to flow freely into the bottom of the box and out the side) and buoyancy terms are not included. The mantle potential temperature at the bottom is assumed to be 1300°C. The first phase solutions (Figures 7a and 7b) reach steady state after about 5000 time steps (approximately 20 and 15 m.y., respectively). Crustal thickness was normalized to the steady state value obtained in this phase for each spreading rate. This normalization is appropriate for we are exploring the range of solutions for each set of boundary and/or buoyancy conditions; also this is done to avoid confusion as the values calculated in this series of modeling runs are not directly comparable with the results of the previous section.

The steady state boundary flow obtained in the first phase then becomes the fixed boundary conditions for the second phase, and buoyancy terms are included. The three branches in the second phase (Figures 7a and 7b) represent three separate calculation runs done for initial mantle temperatures of 1300°C (solid line), 1325°C (dashed line), and 1350°C (dotted line). At the beginning of the second phase there is a large transient increase in crustal thickness that is of greatest magnitude at highest mantle temperatures. These transient increases are much larger in the slow spreading calculations (compare Figures 7a and 7b). The transient increase in crustal thickness reflects the instantaneous incorporation of buoyancy driven flow and are not intended to relate to a natural phenomenon but are instructive in showing the effects controlling flow and melting. As discussed by Scott [1993] and Su and Buck [1993], density changes related to melting (i.e., the change in composition of the solid and retention of melt) affect flow close to the axis. Thermal density variations can affect flow far away from the axis. Thus a change in the boundary conditions primarily changes the thermally driven flow. The transient increase in crustal thickness at the beginning of the second phase of the calculation shows how strongly density variations affect mantle flow and melting of mantle at shallow depths

beneath the ridge axis. The transient increase is followed by a reduction in crustal thickness that is related to another effect of thermally driven flow. Thermal convection leads to cooling of the subridge mantle. This cooling reduces the amount of melt extracted from mantle flowing up below the ridge. Also, cooling increases the viscosity of the mantle and so reduces the buoyancy-driven flow. A steady state is achieved when the mantle has cooled somewhat relative to the inflow temperature.

A transient with more potential for physical meaning occurs in the third phase of the calculation. Here, we have kept the boundary conditions and buoyancy conditions fixed at the final steady state result from the second phase for  $T_m=1300^\circ\text{C}$ . The solid line represents this steady state solution from the end of the second phase (Figures 7a and 7b). The dashed line shows the result for an instantaneous inflow temperature increase to 1325°C, and the dotted line shows the result for 1350°C. Nearly instantaneous inflow temperature increases might occur in nature when a ridge becomes proximal to a hot spot. The effect of a sudden increase in temperature is to cause an initially large increase in the crustal thickness followed by a smaller, steady state change. Again, the effect is much larger at slow spreading rates (Figure 7a) than at fast rates (Figure 7b). Following the transient reduction, the crustal thicknesses once again approach steady state solutions comparable to those determined at the end of the second phase. The range of crustal thicknesses remains much greater for the slow spreading case than the fast spreading case, as we initially determined from the previous steady state calculations (Figure 6).

It is initially surprising that the steady state crustal thicknesses calculated for the case of  $T_m=1300^\circ\text{C}$  at the end of the second and third phases are not only less than the thickness at the beginning of each phase but are also less than the steady state thickness at the end of the first phase even though we allow more driving forces (buoyancy terms) after the first phase (Figures 7a and 7b). This occurs for both the fast and slow spreading cases. To investigate these results, we consider flow depletion patterns for these different steady state solutions for the slow spreading case (Figures 8a and 8b) and compare them with the flow and depletion patterns from our initial series of

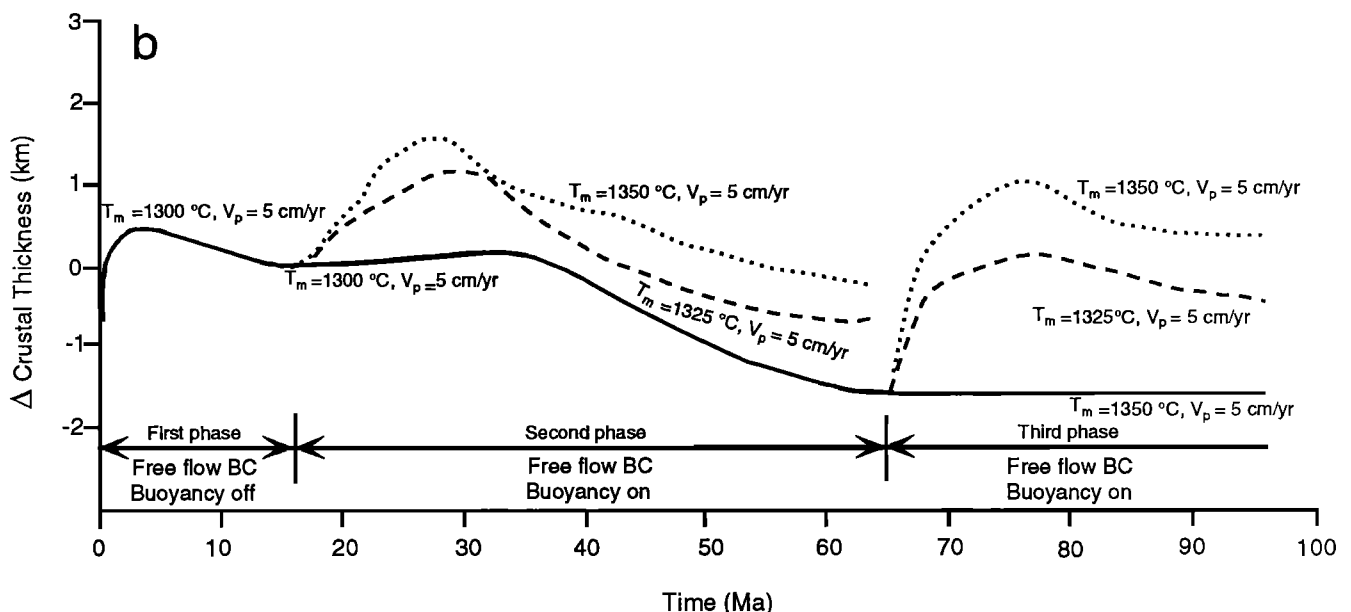


Fig. 7. (continued)

calculations described in the previous section (free flow boundary conditions with buoyancy-driven flow; Figure 8c).

The flow patterns in Figure 8a are driven only by plate separation and basically represent conditions like corner flow. With the inclusion of buoyancy (Figure 8b), the flow becomes more active, and streamlines show that material entering the bottom of the box is focused into a flow boundary layer near the ridge. However, the formation of crust depends not only on the flow pattern but also on the pattern of depletion. Although the same boundary conditions apply for the cases represented in Figures 8a and 8b, the temperature field and hence the pattern of depletion represented in Figure 8b are strongly influenced by buoyancy-driven flow. This can be considered in terms of energy balance; the stronger flow associated with buoyancy results in a greater flow of heat out of the box. Since the inflowing mantle velocity and temperature fields are fixed this causes a net energy loss; resulting in a reduction in the temperature field and consequently in the depletion area. Additionally, the patterns of streamlines in Figures 8a and 8b show that the amount of material entering the depletion area is

different in the two cases. Streamlines can be used to estimate flux. We can see that there is greater flux into the depletion area in Figure 8a than in Figure 8b. This indicates that there is more melt, and hence a thicker crust, formed in the case of Figure 8a (free flow boundary conditions, no buoyancy) compared to that in Figure 8b (fixed flow boundary conditions with buoyancy-driven flow). If we had instead free flow boundary conditions accompanying buoyancy-driven flow (Figure 8c), the energy loss associated with the greater flow of hot material out of the box could be compensated by more material flowing in. In this case, the temperature field could maintain or even increase compared to the case of no buoyancy (Figure 8a).

As noted before, the range of boundary conditions considered here may bracket the effect of temperature changes on crustal thicknesses formed at different rates of seafloor spreading. The details of our results depend on a rather complex interaction between plate-driven flow and buoyancy-driven flow. However, the main conclusions are robust and not dependent on the model boundary conditions.

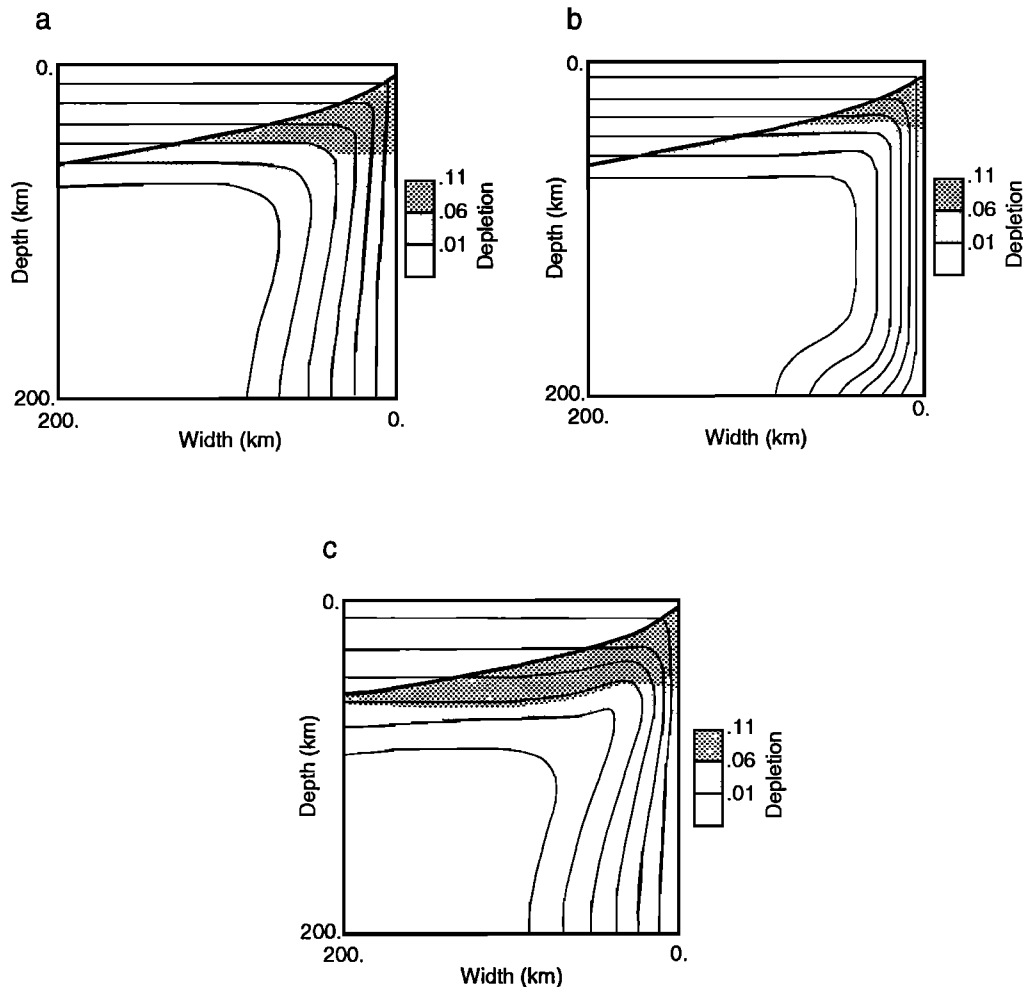


Fig. 8. Flow patterns and the patterns of depletion in slow spreading cases for (a) passive, plate-driven flow with free flow boundary conditions; (b) active, buoyancy, and plate-driven flow with fixed velocity boundary conditions; and (c) active, buoyancy, and plate-driven flow with free flow boundary conditions. The formation of crustal thickness depends on both the flow patterns and the patterns of depletion. Passive flow observed in Figure 8a is like corner flow. Active flow in Figures 8b and 8c show the streamlines focusing toward the ridges. Note different sizes of depletion areas (shaded). The depletion values are related to melting, which is a function of both temperature and pressure. Different boundary conditions affect the temperature field and therefore the size of the depletion area as described further in text.

The large variation in crustal thickness for a small perturbation of mantle temperature at slow spreading ridges may be consistent with recent theoretical work of *Scott* [1993] (Figure 9). *Scott* [1993] defined a variable  $V_c$  as a measure of the convective velocity within 100 km of the ridge axis.  $V_c$  isolates the component of convection due to thermal buoyancy. Figure 9a [from *Scott*, 1993] shows a relationship between  $V_c$  and  $V_p$  (half spreading rate) for a number of different parameter combinations and box sizes in which the calculation was performed. The dotted line is the boundary between strong and weak convection. In the region of strong convection ( $V_c \gg V_p$ ),  $V_c$  increases as  $V_p$  increases, whereas in the region of weak convection ( $V_c \ll V_p$ ),  $V_c$  decreases as  $V_p$  increases. In the transition between these two regions, either situation could occur. That is,  $V_c$  could be an increasing function or a decreasing function of  $V_p$  depending on different box size and parameters selected. In the appendix of *Scott's* [1993] paper, theoretical analysis shows that for strong convection  $V_c \sim V_p^{1/2}$ , whereas for weak convection  $V_c \sim V_p^{-1/2}$ . The amount of melting is related to  $V_c$ , whereas the variations in crustal thickness depend on  $V_c/V_p$ . That is, crustal thickness is a physical quantity related to melt produced per unit of plate separation. We therefore utilize *Scott's* [1993] results and replot them with  $V_c/V_p$  on the vertical axis, reflecting the effect of convective flow on crustal thickness (Figure 9b).  $V_c/V_p$  is always an inverse function of  $V_p$  regardless of viscosity, box size or degree of convection.  $V_c/V_p$  should be proportional to  $V_p^{-1/2}$  and  $V_p^{-3/2}$  for strong and weak convection, respectively, based on *Scott's* [1993] theoretical analysis. This result is consistent with our calculations and indicates that the effect of convection on crustal thickness diminishes as spreading rates increase.

#### AN ATTEMPT TO RECONCILE PREDICTIONS WITH OBSERVATIONS

##### Global Data Set

The theoretically derived curves in Figure 6 appear to exhibit sufficient structure that they should allow a test of the spreading rate dependence of crustal thickness using observational controls. To do this, we need to expand the type of compilation made by *Chen* [1992] and *White et al.* [1992] to include examples of crust that is thicker than the typical oceanic average of 7 km or so. Compilations of crustal thickness estimates that exclude topographic highs [*White et al.*, 1992] that are probably associated with thicker crust are likely to include only crust created in the range of conditions under which its thickness is only weakly dependent on spreading rate and hence cannot provide a suitable test. An expanded compilation was made by *Mutter and Mutter* [1993] in an effort to understand how the internal structure of oceanic crust (the relative proportions of seismic layers 2 and 3) varied as the total thickness increased. The total thickness values from their compilation are also shown in Figure 6. The three dots around crustal thickness of 20 km represent data locations offshore Norway and along the Faeros Iceland Ridge.

The observational data show no more structure than those compiled by *Chen* [1992]. The principal reason is that the effects of mantle temperature and spreading rate, which both influence crustal genesis, cannot be isolated in an analysis of this sort. Also, these data come from a wide variety of locations where mantle conditions may have been very

different. Recall that the curves shown in Figures 6 pertain to one specified value of viscosity and permeability. These curves retain the same form but shift up and down in the theoretical plane depending on the value of these parameters. A comparison of the type shown in Figure 6 cannot be used to establish values of critical mantle parameters.

This result may be of considerable importance as it has been commonly assumed, based on calculations of *McKenzie and Bickle* [1988], *White and McKenzie* [1989], and *Klein and Langmuir* [1987] that crustal thickness values can be used fairly directly to estimate mantle temperatures at the time of crustal formation. Our simple calculations establish that at least spreading rate and preferably also upper mantle viscosity and permeability need to be specified to provide more meaningful estimates of paleotemperatures.

##### Control Data Set

Given that the type of compilation discussed above does not provide an adequate test of the phenomena predicted by the model calculations, we sought data located in an area where spreading rates are known to vary but also within a small enough region that it is reasonable to assume that mantle conditions remained nearly constant. That is, we require a data set for which spreading rate changes might dominate over changes in other parameters and for which crustal thickness estimates are well established. One potentially suitable data set is a high-quality seismic reflection and refraction data set obtained in an area of Mesozoic oceanic crust (Figure 10) adjacent to the Blake Spur Fracture Zone (BSFZ) in the western North Atlantic [*White et al.*, 1990, *Morris et al.*, 1993]. The crust formed 137-155 Ma (magnetic anomalies M14 to M25 [*Klitgord and Schouten*, 1986]). The kinematic history of the central Atlantic is one of long periods of constant spreading and fairly stable poles of motion interrupted by short periods of plate motion changes. A ridge jump occurs at magnetic anomaly M21 time that is reflected in a small kink in the magnetic anomalies along the trace of the fracture zone at 27°25'N latitude [*Klitgord and Schouten*, 1986]. In the western part of the survey area, from magnetic anomaly M21 to M25, the spreading rates were relatively high (19 mm/yr half rate). After anomaly M21, the spreading rate decreased to a half rate of 14 mm/yr, then continued to slow to a half rate of about 9 mm/yr in the eastern part of the survey area [*Kent and Gradstein*, 1985; *Klitgord and Schouten*, 1986].

The data comprise two-ship multichannel seismic reflection and refraction data. The source on *Conrad* was a 10-gun array firing 5821 in.<sup>3</sup> of compressed air on a 40-s schedule and the arrivals were recorded with the *Discovery's* 48-channel, 2.4-km-long streamer which had a group spacing of 50 m. Eighteen expanding spread profiles (ESPs) were acquired of which four are oriented parallel to the paleospreading center. The velocity structures determined from these four ESPs are presented with extensive discussion by *Morris et al.* [1993]. The half spreading rates appropriate to the ESP location are 1.0 cm/yr (ESP 15), 1.2 cm/yr (ESP 16), 1.5 cm/yr (ESP 16), and 1.9 cm/yr (ESP 18).

Estimating total crustal thickness requires a definition of the base of the crust in seismic terms. This boundary is easily recognized as a distinct step to velocity values greater than 8 km/s [*Morris et al.*, 1993] in ESPs 15, 16, and 17 located in the slower spreading crust. In the crust created at the intermediate rate (ESP 18), however, the base of the crust is marked by a

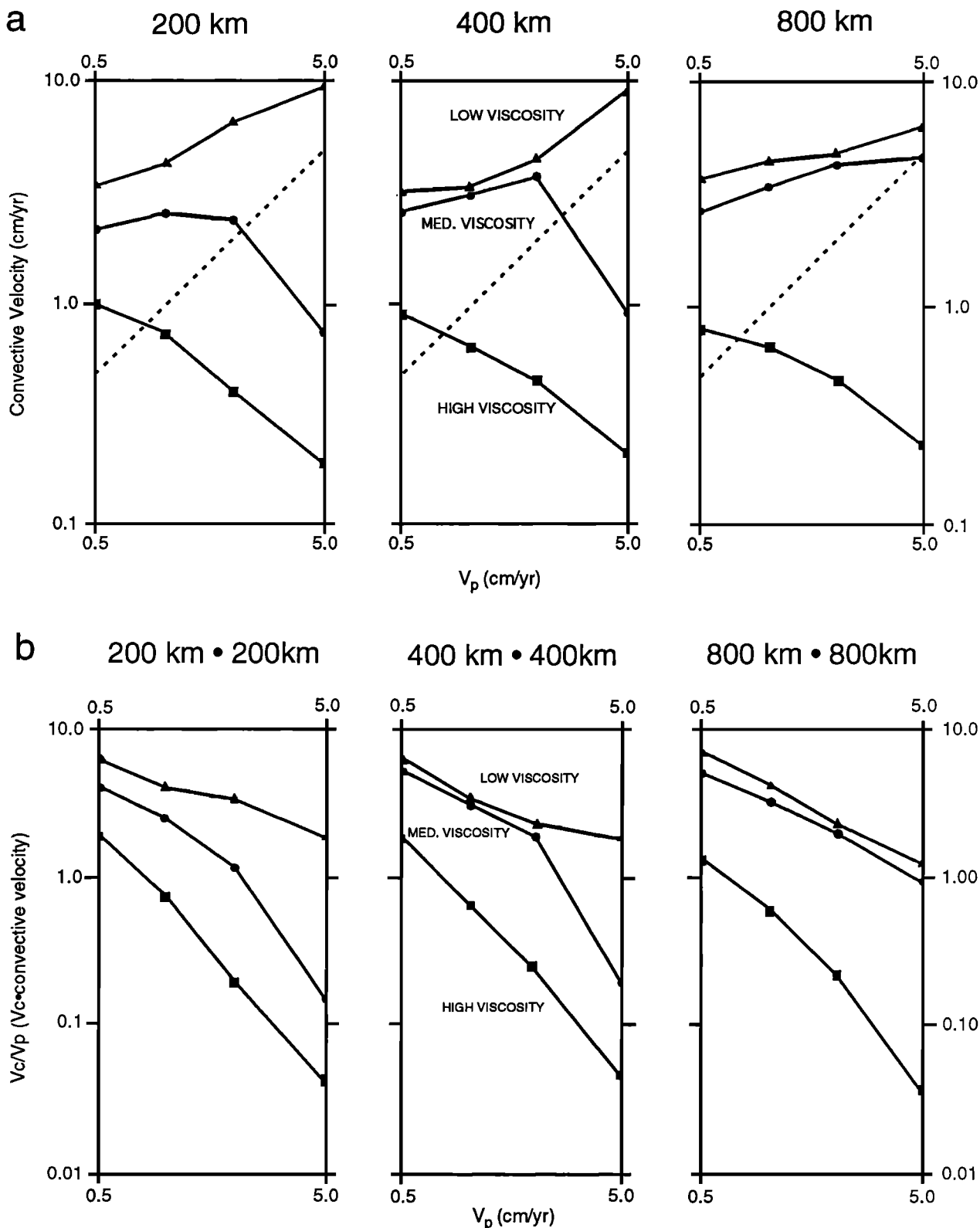


Fig. 9. (a) Convective velocity as a function of plate velocity, viscosity and box size [from Scott, 1993].  $V_c$  (vertical axis) is a measure of the convective velocity within 100 km of the ridge. Horizontal axis is plate velocity ( $V_p$ ) in units of half spreading rate. Dashed lines of  $V_c = V_p$  divide the plots into regimes of weak convection ( $V_c$  decreases with increasing  $V_p$ ) and regimes of strong convection ( $V_c$  increases with increasing  $V_p$ ). In the transition region,  $V_c$  could be an increasing or decreasing function of  $V_p$  depending on box size and parameters selected. Theoretical analysis also shows that for strong convection  $V_c \sim V_p^{1/2}$ , whereas for weak convection  $V_c \sim V_p^{-1/2}$ . (b) Replot of Figure 9a with  $V_c/V_p$  as the vertical axis. Since crustal thickness is a physical quantity related to melt produced per unit of plate separation,  $V_c/V_p$  represents the effect of convective flow on crustal thickness and is always an inverse function of  $V_p$  regardless of viscosity, box size or degree of convection. Based on Scott's [1993] theoretical analysis,  $V_c/V_p$  should be proportional to  $V_p^{-1/2}$  and  $V_p^{-3/2}$  for strong and weak convection, respectively. Scott's [1993] theoretical and numerical results all indicate the effect of buoyancy driven flow on crustal thickness reduce as spreading rates increase, consistent with our results.

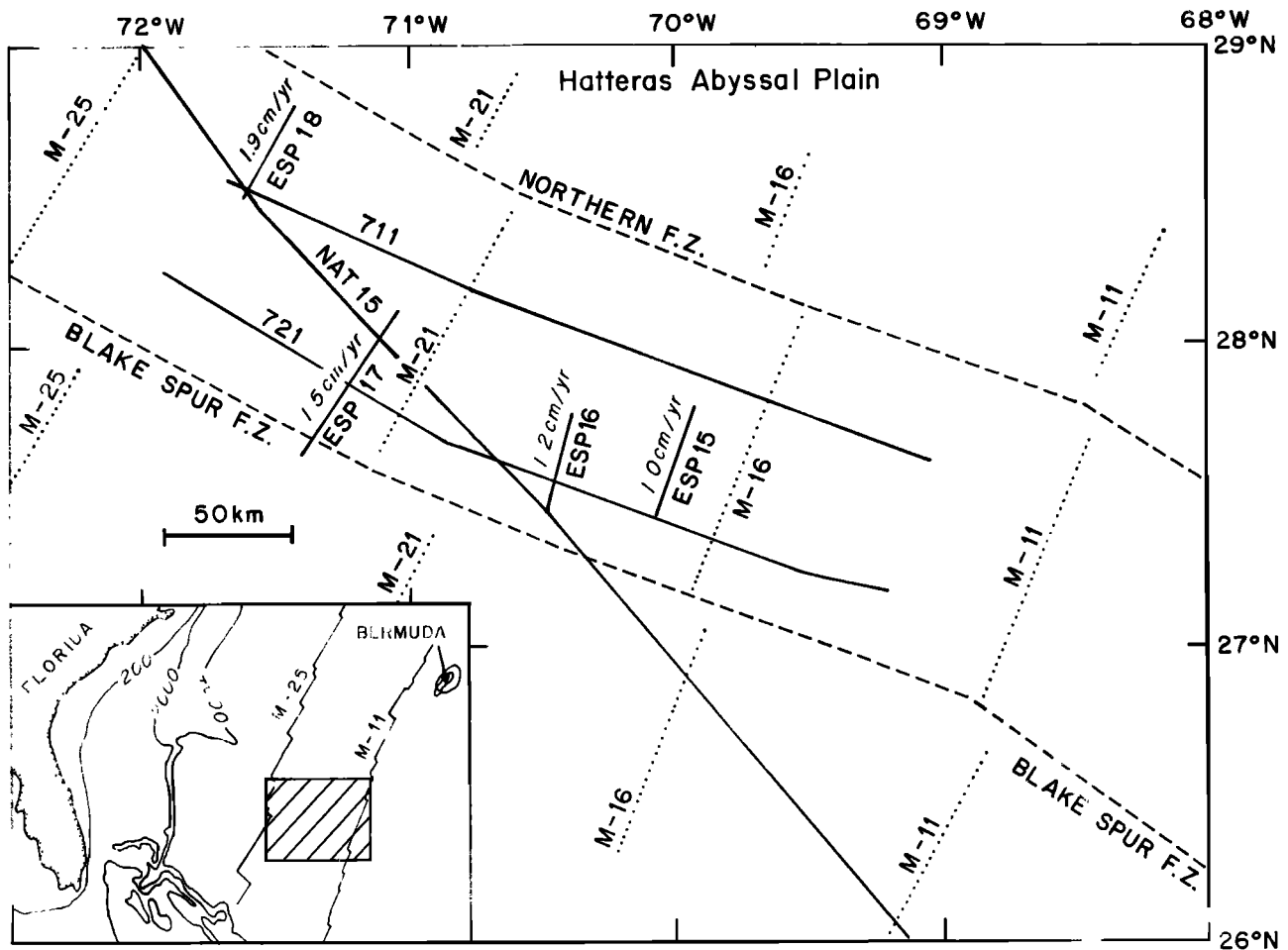


Fig. 10. Track map showing data locations in the Blake Spur area. (Inset shows location of western North Atlantic survey area as shaded box.) Major fracture zones are shown as dashed lines; magnetic lineations are shown as dotted lines. Refraction experiments oriented parallel to the paleospreading center indicated as expanded spread profiles (ESPs) 15-18. Approximate spreading rates [from Kent and Gradstein, 1985] at time of formation of each ESP location are also shown in italics.

Moho transition zone [Morris *et al.*, 1993]. We therefore took two different approaches to estimate the crustal thickness. A minimum thickness is given by taking the depth to the discontinuity where velocity jumps from 7.15 km/s to 7.8 km/s. The maximum is determined by taking the thickness using the location where velocity reaches 8 km/s.

The theoretical relationships together with the observed data from the western North Atlantic are shown in Figure 11. If an average line were passed through the observed thickness values, it would show a slight increase from slow to fast as predicted. Given the variations shown in the observed thickness values, it is clear that the data do not provide a significant substantiation of the model predictions. The observed crustal thicknesses vary by almost a kilometer. The crust at ESP 16 is the most unusual, being considerably thinner than at the other sites. This variation could be attributed to a variety of factors, perhaps even local changes in mantle temperature at the paleo-Mid-Atlantic Ridge. ESP 16 lies deeper than the other three ESPs, and this may indicate that it was produced at lower temperatures. However, at spreading half rates less than about 2 cm/yr the structure of spreading centers is known to be greatly influenced by tectonism, particularly by mechanical extension that could locally thin the crust. Effects of this type cannot easily be factored into our analysis, and the principal conclusion that can be drawn from this example is

only that the observations do not violate model predictions.

We made an extensive search of the literature on crustal structure estimates to establish if suitable data sets for testing the predictions of model calculations exist. Ideally, we require data from regions where the mantle has maintained warmer temperatures and the spreading has varied from slow to intermediate rates. This region must also be small enough that large variations in upper mantle viscosity and permeability are unlikely. We have been unable to locate a suitable data set.

#### CONCLUSIONS

We have established that the effect of buoyancy-driven flow on crustal thickness is more important at slow spreading ridges than that at fast spreading ridges. Therefore small perturbations in mantle temperatures at slow spreading ridges will cause relatively large variations in crustal thickness. This is consistent with the compilation of the observed data.

We can state the conclusion in a number of ways. Although melt produced at fast spreading centers is more abundant than that formed at slow spreading centers, this does not imply that melt produced per unit of separation at fast spreading centers is greater than that at slow spreading rates. One consequence of the interdependent relationship among spreading rate, mantle temperature, and crustal thickness (e.g., Figure 3) is that crust produced at a fast spreading rate may be thicker or thinner than

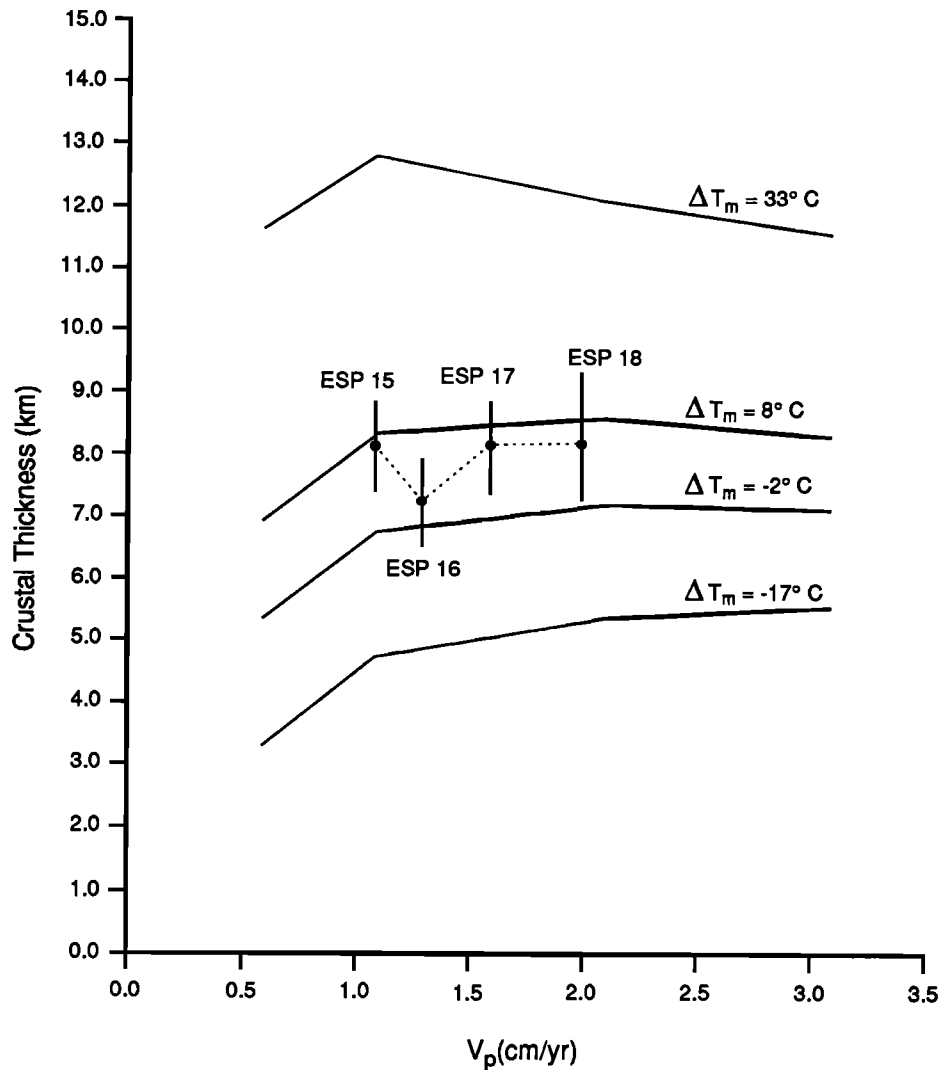


Fig. 11. Theoretical relationships between crustal thickness and spreading rate, together with the observed data from the western North Atlantic. Solid dots represent thickness determinations, solid lines represent uncertainties in these determinations. The crust at ESP 16 is the most unusual, being considerably thinner than at the other sites. While the data are not inconsistent with the model results, they are not conclusive. A more satisfactory test of model predictions will require crustal thickness determinations in a region, where mantle conditions have remained relatively stable while spreading rate has fluctuated over a larger range (e.g., 0.5-3.0 cm/yr, half rate) of spreading rates.

crust produced at slow spreading rates, depending on mantle temperature.

Considered with regard to the production of crustal sections that are thicker than the average value of 7 km or so, our results imply that elevated mantle temperatures are always required to produce thicker crust but that spreading rate becomes an increasingly important factor as average mantle temperatures increase (e.g., Figure 6). At elevated mantle temperatures, a reduction in spreading rates can increase the thickness of crust by about 25%. This increase can be considered relative to that produced by passive upwelling alone. If crustal thickness values are used to infer mantle temperature at the time of crustal genesis using a passive upwelling model, mantle temperatures will be systematically overestimated unless spreading rates are very high.

One caveat to the discussion above is that a variety of parameters that describe the properties of the mantle have a

significant influence on the relationship between crustal thickness, spreading rate and mantle temperature. We investigated the effect of viscosity and permeability on crustal genesis because both of these affect buoyancy-driven flow and convection. We found that the form of the relationships do not change but that derived values of crustal thickness changed considerably. The present uncertainty in upper mantle viscosity and permeability is quite large, this further limiting attempts to derive meaningful estimates of mantle temperature from crustal thickness values.

Finally, one result from our investigation is that regional data sets of high-quality seismic measurements that could be used to test the predictions of theoretical calculations apparently need to be acquired. Data from the Blake Spur Fracture Zone area provided only a limited test that suggests that theory and observation are not in conflict. However, they do not establish a satisfactory test of the predictions.

**Acknowledgments.** This work was supported by NSF grants OCE89-12004 and OCE90-12781. Discussions with D. Sparks were helpful. Reviews by J. Hopper, J-C Sempere, and two anonymous individuals significantly improved the content and organization of the paper. N. Katz provided assistance in graphic presentations. J. Graney provided editorial and technical assistance. This is Lamont-Doherty Earth Observatory contribution No. 5146.

#### REFERENCES

- Borch, R.C., and H.W. Green, Experimental investigation of the rheology and structure of partially molten lherzolite deformed under upper mantle pressures and temperatures (abstract), *Eos Trans. AGU*, *71*, 629, 1990.
- Buck, W.R., and W. Su, Focused mantle upwelling below mid-ocean ridges due to feedback between viscosity and melting, *Geophys. Res. Lett.*, *16*, 641-644, 1989.
- Cheadle, M.J., Properties of texturally equilibrated two-phase aggregates, Ph.D. thesis, 156 pp., Univ. of Cambridge, Cambridge, England, 1989.
- Chen, Y.J., Oceanic crustal thickness versus spreading rate, *Geophys. Res. Lett.*, *19*, 753-756, 1992.
- Cordery, M.J., and J. Phipps Morgan, Convection and melting at mid-ocean ridges, *J. Geophys. Res.*, *98*, 19,477-19,503, 1993.
- Kent, D.V., and F.M. Gradstein, A Cretaceous and Jurassic geochronology, *Geol. Soc. Am. Bull.*, *96*, 1419-1427, 1985.
- Klein, E.M., and C.H. Langmuir, Ocean ridge basalt chemistry, axial depth, and crustal thickness and temperature variation in the mantle, *J. Geophys. Res.*, *92*, 8089-8115, 1987.
- Klitgord, K.D., and H. Schouten, Plate kinematics of the central Atlantic, in *The Geology of North America*, vol. M, *The Western North Atlantic Region*, edited by P.R. Vogt and B.E. Tucholke, pp.351-378, Geological Society of America, Boulder, Co., 1986.
- Macdonald, K. C., Mid-ocean ridges: Fine scale tectonic, volcanic, and hydrothermal processes within the plate boundary zone, *Annu. Rev. Earth Planet. Sci.*, *10*, 155-190, 1982.
- McKenzie, D., and M. J. Bickle, The volume and composition of melt generated by extension of the lithosphere, *J. Petrol.*, *29*, 625-679, 1988.
- Morris, E., R.S. Detrick, T.A. Minshull, J.C. Mutter, R.S. White, W. Su, and P. Buhl, Variations in seismic structure of Mesozoic aged crust in the western North Atlantic, *J. Geophys. Res.*, *98*, 13,879-13903, 1993.
- Mutter, C.Z., and J.C. Mutter, Variations in thickness of layer 3 dominate oceanic crustal structure, *Earth Planet. Sci. Lett.*, *117*, 295-317, 1993.
- Oxburgh, E.R., Heat flow and magma genesis, in *Physics of Magmatic Process*, edited by R.B. Hargraves, pp. 161-199, Princeton University Press, Princeton, N. J., 1980.
- Parsons, B., and J.G. Sclater, An analysis of the variation of ocean floor bathymetry and heat flow with age, *J. Geophys. Res.*, *82*, 803-827, 1977.
- Phipps Morgan, J., melt migration beneath mid-ocean spreading centers, *Geophys. Res. Lett.*, *14*, 1238-1241, 1987.
- Reid, I., and H.R. Jackson, Oceanic spreading rate and crustal thickness, *Mar. Geophys. Res.*, *5*, 165-172, 1981.
- Ribe, N.M., The deformation and compaction of partially molten zones, *Geophys. J.R. Astron. Soc.*, *83*, 487-501, 1985.
- Richter, F.M., and D. McKenzie, Simple models of mantle convection, *J. Geophys.*, *44*, 441-471, 1984.
- Scott, D.R., Small-scale convection and mantle melting beneath mid-ocean ridges, in *Mantle Flow and Melt Generation at Mid-Ocean Ridges*, *Geophys. Monogr.*, Ser. vol. 71, pp. 327-352, AGU, Washington, D.C., 1993.
- Scott, D.R., and D.J. Stevenson, A self-consistent model of melting, magma migration, and buoyancy-driven circulation beneath a mid-ocean ridge, *J. Geophys. Res.*, *94*, 2973-2988, 1989.
- Sotin, C., and E.M. Parmentier, Dynamical consequences of compositional and thermal density stratification beneath spreading centers, *Geophys. Res. Lett.*, *16*, 835-838, 1989.
- Spiegelman, M., and D.P. McKenzie, Simple 2-D models for melt extraction at mid-ocean ridges and island arcs, *Earth Planet. Sci. Lett.*, *83*, 137-152, 1987.
- Su, W., and R.W. Buck, Buoyancy effects on mantle flow under mid-ocean ridge, submitted to *J. Geophys. Res.*, *98*, 12,191-12,205, 1993.
- White, R.S., Atlantic oceanic crust: Seismic structure of a slow spreading ridge, in Ophiolites and the Oceanic Lithosphere, *Geol. Soc. Spec. Publ. London*, *13*, 34-44, 1984.
- White, R. S., and D. P. McKenzie, Magmatism at rift zones: The generation of volcanic continental margins and flood basalts, *J. Geophys. Res.*, *94*, 7685-7729, 1989.
- White, R.S., R.S. Detrick, J.C. Mutter, P. Buhl, T.A. Minshull, and E. Morris, New seismic images of oceanic crustal structure, *Geology*, *18*, 462-465, 1990.
- White, R. S., D. McKenzie, and R. K. O'Nions, Oceanic crustal thickness from seismic measurements and rare earth element inversions, *J. Geophys. Res.*, *97*, 19,683-19,715, 1992.

W. R. Buck, C. Z. Mutter, J. C. Mutter, and W. Su, Lamont-Doherty Earth Observatory, Palisades, NY 10964.

(Received November 6, 1992;  
revised October 5, 1993;  
accepted October 20, 1993.)